Available online at www.sciencedirect.com
SCIENCE DIRECT®
International Journal of Heat and Mass Transfer 48 (2005) 4481–4491
International Journal of HEAT and MASS TRANSFER
www.elsevier.com/locate/ijhmt

Partly three-dimensional global modeling of a silicon Czochralski furnace. I. Principles, formulation and implementation of the model

Lijun Liu, Koichi Kakimoto *

Research Institute for Applied Mechanics, Kyushu University, 6-1, Kasuga-Koen, Kasuga 816-8580, Japan

Received 8 June 2004; received in revised form 30 March 2005
Available online 19 July 2005

Abstract

A novel model for three-dimensional (3D) global simulation of heat transfer in a Czochralski (CZ) furnace for silicon crystal growth was proposed. Convective, conductive and radiative heat transfers in the furnace are solved together in a conjugated way by a finite control-volume method. A mixed 2D/3D space discretization technique was developed, and concepts of 2D domain and 3D domain for a CZ furnace were proposed. This technique enables 3D global simulations to be conducted with moderate requirements of computer memory and computation time. A 2D global simulation was carried out to obtain good initial conditions for 3D global modeling to speed up the global iteration. The model was demonstrated to be valid and reasonable.

Keywords: Computer simulation; Global modeling; Czochralski method; Radiation; Semiconducting silicon

1. Introduction

The Czochralski (CZ) method has for several decades been the most widely used technique for growing high-quality bulk crystals of silicon. The thermal field in the as-grown crystal, the melt–crystal interface shape and the melt flow motion in the crucible have significant effects on the formation of micro-defects and crystal quality in a CZ growth process. It is therefore important to elucidate the heat and mass transfer mechanisms and to establish methods for controlling the melt–crystal interface shape and the thermal field in a CZ furnace. With the increasing capacity of modern computer and computation technology, application of numerical simulation has become an effective and essential tool for field prediction, parameter control and design optimization of a CZ growth system in order to improve silicon crystal quality.

Over the past two decades, there have been many works on numerical analyses of CZ crystal growth processes using various models that can be generally divided into three types: local models [1–4], 2D global models [5–8] and 2D global/3D local combined models [9,10]. In fact, since all constituents of a CZ furnace are closely related to each other through different forms of heat transfer by melt convection, solid conduction and thermal radiation, the CZ growth furnace is a highly nonlinear and strongly conjugated thermal system.

* Corresponding author. Tel.: +81 92 583 7741; fax: +81 92 583 7743.
E-mail address: kakimoto@riam.kyushu-u.ac.jp (K. Kakimoto).

0017-9310/$ - see front matter © 2005 Elsevier Ltd. All rights reserved.
doi:10.1016/j.ijheatmasstransfer.2005.04.031

Nomenclature

c	heat capacity (J/kg K)
$\vec{F}$	body force exerted on melt by external field imposed (N/m^3)
$\vec{g}$	gravitational acceleration (m/s^2)
ΔH	release of the latent heat of solidification (J/kg)
k	thermal conductivity (W/m K)
K	surface view factor between two infinitesimal radiative elements
K_C	axisymmetric view factor
K_e	surface view factor between two finite radiative elements
$\vec{n}$	unit normal vector
p	pressure (Pa)
pr	circumferential projection
q	heat flux (W/m^2)
$\vec{r}$	space vector (m)
s	longitudinal coordinate (m)
S	area (m^2)
T	temperature (K)
T_m	melting temperature of silicon (K)
$\vec{V}$	velocity (m/s)
V_g	crystal growth rate (m/s)
∂V	radiative enclosure
∂V^2	the part of radiative enclosure in the 2D domain
∂V^3	the part of radiative enclosure in the 3D domain
$\vec{x}, \vec{x}^*$	infinitesimal radiative surface elements
$\vec{x}'$	infinitesimal radiative elements in the projection plane
X, X_i, X_{ji}	finite radiative surface elements

Greek symbols

β_T	thermal expansion coefficient (1/K)
ε	radiative emissivity
μ	melt viscosity (kg/m s)
θ, θ^*	azimuthal angles
ρ	density (kg/m^3)
σ	Stefan–Boltzmann constant (W/m^2 K^4)

Subscripts

c	geometrical center
h	heater
m	melt
rad	radiation
s	solid
S	skeleton of the global domain

Knowledge of heat transport throughout the entire furnace is thus required. On the other hand, the melt flow in a crucible and, hence, the thermal field within the growth furnace are principally three-dimensional, especially in cases with melt flow of a high Reynolds number or under the influence of external fields. Therefore, 3D global analysis of a CZ growth system is necessary for a better understanding of realistic phenomena and insight physics of the growth process and, hence, for process improvement. Unfortunately, however, although there have been many studies on local simulations and 2D global simulations, as mentioned above, there has been no report on real 3D global simulations.

As far as a 3D global simulation is concerned, the most challenging difficulties lie in the requirements of very large computer memory and very long time for computation. In particular, in the calculation of radiative heat transfer, both the computer memory and the computation time are proportional to the square of the total number of radiation elements in the growth system. In this paper, some numerical techniques have been developed for computation and some novel measures have been taken in establishing a 3D global model in order to overcome these difficulties. First, a multi-block structured grid system has been used for space discretization, and a finite control-volume method has been employed for equation discretization. Some efficient algorithms based on a structured mesh can thus be used to speed up the computation. Second, 2D global simulation has been performed at the outset of computation in order to obtain better initial fields and values of unknown parameters a priori, such as heater power and melt–crystal interface shape. The third but the most important technique developed is a 2D/3D mixed discretization technique in which the domains at the core region of a furnace are discretized in a three-dimensional way and the other domains are discretized in a two-dimensional way. By applying these numerical techniques and simplification measures, 3D global simulations are feasible with moderate requirements of computation resources.

2. Model description and discrete system

2.1. Major assumptions and definitions

A typical configuration of a Czochralski growth furnace, which will serve as a basis for illustrating our model and method in later sections, is shown in Fig. 1(a).

The following major assumptions are used in our model: (1) The geometry of the furnace configuration

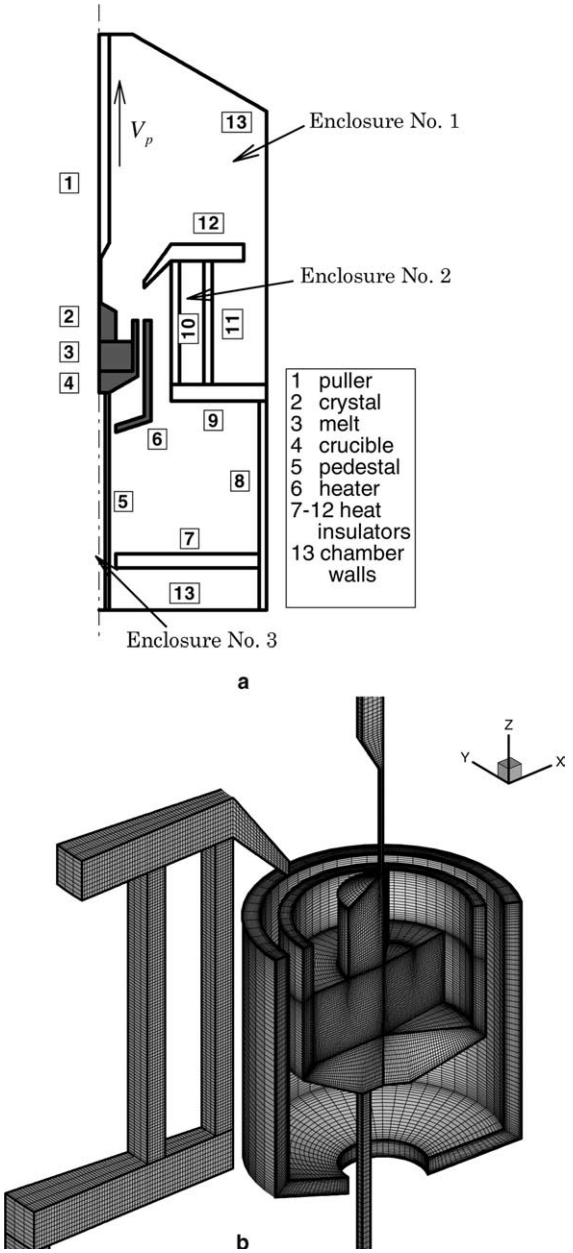

Fig. 1. Discrete system of computation: (a) Configuration and domain partition of a typical Czochralski furnace: 3D domain (shadowed) and 2D domain (non-shadowed), (b) a local view of the computation grid.

is axisymmetric with the exception of the melt–crystal interface, whose shape might be three-dimensional. (2) The growth system is quasi-steady. (3) Radiative transfer is modeled as diffuse-gray surface radiation. (4) The melt flow in the crucible is laminar and incompressible. (5) The effect of gas flow in the furnace is neglected. Furthermore, since our purpose is to develop a 3D global model, the capillary effect of the melt free surface is neglected for the sake of simplicity.

According to heat transport mechanisms in different media and their implementations in the algorithm, we subdivide all of the constituents of a growth furnace into three types of media: radiative enclosure macro-elements, the melt–crystal macro-element and solid conductive macro-elements. The radiative enclosures connect the various liquid and solid constituents in the furnace. Heat is exchanged by radiation between surfaces of a radiative enclosure. The melt–crystal macro-element consists of the melt and the crystal together with their interface, whose shape is unknown a priori. The thermal field in the melt–crystal macro-element is governed by the convective heat transfer in the melt and the conductive heat transfer in the crystal. The solid conductive macro-elements cover all the other solid components in a furnace in which the heat transfer is in the form of conduction (and advection if it is rotating). Among them, the chamber walls are a special solid conductive macro-element that can be treated in one dimension. The set of interfaces connecting different macro-elements constitutes the skeleton of the global domain. Obviously, it consists of two types of interfaces: the radiative surfaces of the radiative enclosures and the conductive interfaces between adjacent solid conductive macro-elements or the melt–crystal macro-element. The global model consists of a set of local iterations for each of these macro-elements and a global conjugated iteration among them through iteratively updating the thermal field on the skeleton of the global domain.

2.2. Construction of a discrete system

In order to establish a discrete system for numerical simulation, the domains of all constituents of a furnace are subdivided into a number of block regions, for example, as shown in Fig. 1(a), in which subdivision resulted in a total of 13 block regions. Each of these block regions represents a conductive macro-element except for block number 2 and block number 3, which constitute the melt–crystal macro-element. All of the radiative surfaces of these block regions constitute the radiative enclosure macro-elements in the furnace. There are three radiative enclosures in the example shown in Fig. 1(a). A structured mesh is generated for each of these block regions, while the chamber walls are discretized in one dimension.

Since the most challenging difficulty in 3D global modeling is the requirements of very large computer memory and very long calculation time, measures to simplify the model must be taken. We therefore developed a mixed 2D/3D discretization technique. In this technique, the domains of components in the core region of a furnace, for example, the melt, crystal, crucible and heater, as marked by a shadow in Fig. 1(a), are

discretized in a three-dimensional way. The remaining domains that are away from the core region are discretized in a two-dimensional way. This technique is based on (1) the fact that the three-dimensionality of the system is induced originally in the melt flow and (2) the observation that it rapidly becomes weaker with increase in distance from the melt region and finally nearly disappears at the chamber walls that are cooled by external coolant convection. We can thus assume that the core region of a CZ growth furnace, namely, the 3D domain, is characterized by three-dimensionality and that the regions away from the core region, namely, the 2D domain, are predominantly two-dimensionally. The thermal field is uniform in the azimuthal direction in the 2D domain, and we can therefore treat them in two dimensions in local iterations.

Whether a component or a macro-element is included in the 2D domain or in the 3D domain depends on the available computer memory and permissible computation time as well as the expected extent of uniformity of the thermal field in the azimuthal direction. The number of macro-elements or components included in the 3D domain is selectable and the external boundaries of the 3D domain are adjustable in the model. Therefore, the proposed 3D global model turns out to be a 2D axisymmetric global model when the growth system is two-dimensionally governed or a fully 3D global model when it is entirely three-dimensionally featured.

As a result, for example, a local view of the computation grid system is as shown in Fig. 1(b) where the 3D domain includes the crystal, melt, crucible and heater. For the sake of flexibility, we programmed our code in a 3D frame for local iterations in all macro-elements. An optimum sector domain of five degrees is selected for space discretization for any macro-element in the 2D domain. Three columns of control volume are distributed in the circumferential direction to represent the local geometry of the configuration for geometrical coefficient calculation. However, the governing equations are discretized and solved for the center column only.

The multi-block 3D-structured grid system is established in such a way that the circumferential projection of the 3D mesh in a meridional plane is a multi-block 2D-structured grid system, which is to be used in 2D global simulation for obtaining better initial fields and parameter values. The grids of adjacent 2D or 3D blocks are consistent with each other along their interfaces. For radiation calculations, the chamber walls are discretized in one dimension, while on other radiative surfaces, the finite radiative surface elements are also consistent with the surface grids of solid or liquid regions to which the radiative surface belongs. By doing so, the manipulations become simple and efficient when information is transferred from the 2D global solution to 3D global simulation or when information is exchanged between two adjacent macro-elements.

By applying these measures, the total numbers of discrete control volumes and the radiative surface elements decrease dramatically, enabling 3D global modeling with moderate requirement of computer resources and permissible computation time. Furthermore, in order to improve the preciseness of computation, the grids are refined with special attention to places close to interfaces or boundaries, to places with abrupt changes in physical properties or large gradient of variable field, and to sharp edges or corners. This is particularly important for the radiation calculation in which the calculation of view factors at edges or corners is very sensitive to the grid quality close to them.

3. Radiative heat transfer in radiative enclosures

Modeling of radiative heat transfer in radiative enclosures is an important part of global simulation. In our model, the radiative heat exchange is modeled on the basis of an assumption of diffuse-gray surface radiation. A net-radiation approach [6] is employed for the radiation calculation. Each radiative surface element distributed on the enclosure is taken as an isothermal patch. The view factor associated with every pair of radiative surface elements is first calculated, taking into account the viewed and hidden parts of the enclosure. A matrix relationship is then established and solved by iteration between the net heat fluxes and the radiative emitted heat fluxes, i.e., the fourth powers of temperatures, on the enclosure surfaces.

Let ∂V stand for a radiative enclosure. The surface temperature $T(\vec{x})$ and the net heat flux $q(\vec{x})$ on ∂V are related by the following integral relationship:

$$\frac{q(\vec{x})}{\varepsilon(\vec{x})} - \int_{\vec{x}^*\in\partial V} K(\vec{x},\vec{x}^*)\frac{1-\varepsilon(\vec{x}^*)}{\varepsilon(\vec{x}^*)}q(\vec{x}^*)\,\mathrm{d}S^* = \sigma T^4(\vec{x}) - \int_{\vec{x}^*\in\partial V} K(\vec{x},\vec{x}^*)\sigma T^4(\vec{x}^*)\,\mathrm{d}S^*, \quad (1)$$

where $\vec{x}$ and $\vec{x}^*$ are infinitesimal radiative surface elements on ∂V. $\mathrm{d}S^*$ is the area of the infinitesimal surface element $\vec{x}^*$. $K(\vec{x},\vec{x}^*)$ is the surface view factor between $\vec{x}$ and $\vec{x}^*$. Whenever $\vec{x}$ and $\vec{x}^*$ face each other, it is given by the following formula:

$$K(\vec{x},\vec{x}^*) = -\frac{[(\vec{x}-\vec{x}^*)\cdot\vec{n}][(\vec{x}-\vec{x}^*)\cdot\vec{n}^*]}{\pi[(\vec{x}-\vec{x}^*)\cdot(\vec{x}-\vec{x}^*)]^2}. \quad (2)$$

Otherwise, when $\vec{x}$ and $\vec{x}^*$ do not face each other, it equals zero.

In 2D global modeling, the system is governed by two-dimensional physics. Let $pr(\partial V)$ stand for the intersection of ∂V and a meridional plane $\theta = 0$, as illustrated in Fig. 1(a), and s be the curvilinear abscissa along it. The radiation calculation is performed on $pr(\partial V)$ that is discretized by a set of one-dimensional finite elements.

Let X and X_i represent the finite elements on $pr(\partial V)$, and let $\vec{x}_c$ and $\vec{x}_{ic}$ denote their geometrical centers respectively. The discretized form of relationship (1) is obtained as follows after some manipulations by taking into account the axisymmetry of the furnace:

$$\frac{q(X)}{\varepsilon(X)} - \sum_{i=1}^{NT} r_{ic} K_C(\vec{x}_c, \vec{x}_{ic}) \frac{1-\varepsilon(X_i)}{\varepsilon(X_i)} q(X_i) \Delta s_i = \sigma T^4(X) - \sum_{i=1}^{NT} r_{ic} K_C(\vec{x}_c, \vec{x}_{ic}) \sigma T^4(X_i) \Delta s_i. \quad (3)$$

Matrix Eq. (3) is solved in the 2D global modeling for a radiative enclosure, in which NT is the total number of finite radiative elements distributed on it.

The axisymmetric view factor $K_C(\vec{x}_c, \vec{x}_{ic})$ is defined by the integral

$$K_C(\vec{x}_c, \vec{x}_{ic}) = \int_0^{2\pi} K(\vec{x}_c, \vec{x}^*_{ic})\, d\theta^*, \quad (4)$$

where $\vec{x}^*_{ic} = (r_{ic}\cos\theta^*, r_{ic}\sin\theta^*, z_{ic})$.

In 3D global modeling, let ∂V^2 and ∂V^3 denote the radiative surfaces of a radiative enclosure that fall in the 2D domain and 3D domain, respectively, as illustrated in Fig. 2. Taking into account the structure of the discrete system, the two-dimensional physics in the 2D domain and the axisymmetry of the furnace, the discretized form of relationship (1) is obtained as follows for any finite radiative element $\vec{X} \in \partial V$, after many trivial manipulations:

$$\frac{q(X)}{\varepsilon(X)} - \sigma T^4(X) = \sum_{j=1}^{M_{V2}} \left[\frac{1-\varepsilon(X_j)}{\varepsilon(X_j)} q(X_j) - \sigma T^4(X_j)\right] K_C(\vec{x}_c, \vec{x}_{jc}) r_{jc} \Delta s_j + \sum_{j=1}^{M_{V3}} \sum_{i=1}^{N_j} \left[\frac{1-\varepsilon(X_{ji})}{\varepsilon(X_{ji})} q(X_{ji}) - \sigma T^4(X_{ji})\right] \times K_e(X, X_{ji}) r_{jic} \Delta s_{ji}. \quad (5)$$

M_{V2} and M_{V3} are the total numbers of radiative elements along $pr(\partial V^2)$ and $pr(\partial V^3)$, while N_j is the total element number in the azimuthal direction at $\vec{x}'_{jic} \in pr(\partial V^3)$. The space relationship of the related surface elements is illustrated in Fig. 2(a) when $X \in \partial V^2$ and in Fig. 2(b) when $X \in \partial V^3$.

The view factor $K_e(X, X_{ji})$ is calculated as follows:

$$\text{when } \vec{X} \in \partial V^2,\ K_e(X, X_{ji}) = \frac{(\theta_{ji2} - \theta_{ji1})}{2\pi} K_C(\vec{x}_c, \vec{x}_{jic}), \quad (6)$$

$$\text{when } \vec{X} \in \partial V^3,\ K_e(X, X_{ji}) = \int_{\theta_{ji1}}^{\theta_{ji2}} K(\vec{x}_c, \vec{x}^*_{jic})\, d\theta^*, \quad (7)$$

where $(\theta_{ji1}, \theta_{ji2})$ is the azimuth range covered by $X_{ji} \in \partial V^3$ and $\vec{x}^*_{jic} = (r_{jic}\cos\theta^*, r_{jic}\sin\theta^*, z_{jic})$.

Eq. (5) is applied to every radiative surface element of a radiative enclosure. The resulting matrix equation is solved by a local iterative procedure. Since there are two unknowns but only one equation for a radiative element, either the net heat flux or the temperature of a radiative element is kept unchanged, while another unknown is iteratively solved. The unchanged unknown will be renewed and solved in the global iteration. For example, in our calculation, the following conditions are applied in the local iterations of radiation calculations for each radiative enclosure of a growth furnace. On the inside wall of heater,

$$q(X) = q_S(X) \quad (8)$$

and on the other radiative surfaces of a radiative enclosure,

$$T(X) = T_S(X). \quad (9)$$

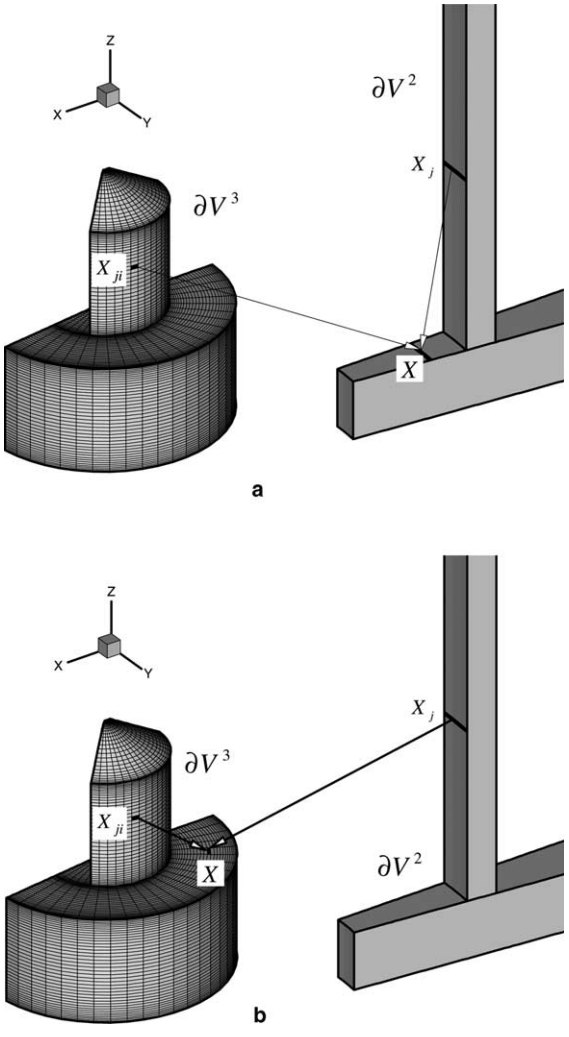

Fig. 2. Space relationship of radiative surface elements: (a) $X \in \partial V^2$, (b) $X \in \partial V^3$.

Here, $q_S(X)$ and $T_S(X)$ are the outgoing heat flux and the temperature on the skeleton of the global domain of a furnace, respectively. They are renewed and solved in the global iteration but kept fixed in local iterations of any macro-elements.

The accuracy of the radiation calculation is checked with the help of the energy conservation in a radiative enclosure, i.e.,

$$\oiint_{\partial V} q(\vec{x})\,\mathrm{d}S = 0. \tag{10}$$

In our calculations, the magnitude of the left side of formulation (10) is less than 0.02% of the heater power.

Another important task in modeling radiative heat transport in a radiative enclosure is the calculation of view factors. Atherton et al. [5] found that the error of view factor calculation was more sensitive to the azimuthal than to the axial or radial discretization by a numerical integration approach. In our calculations, the preciseness of the view factor calculation is ensured by two measures. First, fine resolution of radiative element distribution is ensured at locations where shape changes of configuration geometry or discontinuities of view factors exist. Second, the integrations in the azimuthal direction in formulations (4) and (7) are solved analytically as follows.

By noting the similar forms of expression in formulations (4) and (7), we first consider a general integral $\int_0^{\theta} K(\vec{x}_c,\vec{x}^*)\,\mathrm{d}\theta^*$, in which $\vec{x}_c = (r_c\cos\theta_c, r_c\sin\theta_c, z_c)$ and $\vec{x}^* = (r'\cos\theta^*, r'\sin\theta^*, z')$. The circumferential projection of $\vec{x}^*$ in plane $\theta^* = 0$ (or named the projection plane) is $\vec{x}' = (r', 0, z')$.

Substituting the expressions of $\vec{x}_c$, $\vec{x}^*$, $\vec{n}_c$ and $\vec{n}^*$ into the formulation of $K(\vec{x}_c,\vec{x}^*)$, like expression (2), and then integrating it with respect to θ^* over $(0,\theta)$, we can finally obtain the following analytical expression after many trivial manipulations:

$$\int_0^{\theta} K(\vec{x}_c,\vec{x}^*)\,\mathrm{d}\theta^* = I(\theta), \tag{11}$$

where $I(\theta)$ is a function with respect to θ only. It was not developed here in detail for brevity.

Now let us consider the calculation of the axisymmetric view factor $K_C(\vec{x}_c,\vec{x}')$. Let Θ be the range of θ^* for which $\vec{x}_c$ and $\vec{x}^*$ face each other and, without loss of generality, characterize it as a set of m_C intervals $]\theta_{km},\theta_{kM}[$, i.e.,

$$\Theta = \bigcup_{k=1}^{m_C}]\theta_{km},\theta_{kM}[, \quad 0 \leqslant \theta_{km} < \theta_{kM} \leqslant 2\pi. \tag{12}$$

Applying formulations (11) and (12), the axisymmetric view factor gives

$$K_C(\vec{x}_c,\vec{x}') = \sum_{k=1}^{m_C} [I(\theta_{kM}) - I(\theta_{km})]. \tag{13}$$

$\Theta$is calculated by a view and hidden algorithm [6].

Regarding the calculation of the view factor between two finite surface elements as expressed in formulation (7), the range of $\theta^* \in]\theta_{ji1},\theta_{ji2}[$ for which $\vec{x}_c$ and $\vec{x}^*_{jic}$ face each other is calculated as

$$\Lambda = \Theta \bigcap]\theta_{ji1},\theta_{ji2}[, \tag{14}$$

Λcan also be characterized by a set of m_e intervals $]\theta_{ke},\theta_{kE}[$, i.e.,

$$\Lambda = \bigcup_{k=1}^{m_e}]\theta_{ke},\theta_{kE}[, \quad \theta_{ji1} \leqslant \theta_{ke} < \theta_{kE} \leqslant \theta_{ji2}. \tag{15}$$

Applying formulations (11) and (15), the view factor in formulation (7) gives

$$K_e(X,X_{ji}) = \sum_{k=1}^{m_e} [I(\theta_{kE}) - I(\theta_{ke})]. \tag{16}$$

By this procedure, all view factors in Eq. (5) are calculated analytically and precisely.

4. Convective heat transfer in the melt and conductive heat transfer in solid constituents

The melt–crystal macro-element is a union of the melt and the crystal. A local iteration is performed in this combined domain in order to ensure the thermal conditions on the melt–crystal interface are satisfactorily met throughout the global iteration, in which the temperature along the melt–crystal interface will be used in tracking the interface location. In the local iteration, however, the interface is kept fixed.

With the assumptions of a quasi-steady system and incompressible laminar flow of the melt, the mass conservation, momentum and energy equations for the melt flow in a crucible can be written as follows:

$$\nabla\cdot\vec{V} = 0, \tag{17}$$

$$\rho\vec{V}\cdot\nabla\vec{V} = -\nabla p + \nabla\cdot\left[\mu(\nabla\vec{V} + \nabla\vec{V}^{\mathrm{T}})\right] - \rho\vec{g}\beta_{\mathrm{T}}(T - T_{\mathrm{m}}) + \vec{F}, \tag{18}$$

$$\rho c\vec{V}\cdot\nabla T = \nabla\cdot(k\nabla T). \tag{19}$$

The last two terms in Eq. (18) are the thermal buoyancy force and the body force exerted on the melt by external fields that might be imposed.

The governing equation for heat transfer in the crystal is:

$$\rho_s c_s V_p\vec{e}_z\cdot\nabla T = \nabla\cdot(k_s\nabla T). \tag{20}$$

For the calculation of melt flow, a non-slip condition is applied on all crucible walls and the crystal solidification front. A free surface condition is enforced on the melt top surface. For the calculation of thermal field,

the boundary conditions are given as follows. On the melt–crucible interfaces and the crystal–seed interface, where heat is transferred by conduction,

$$T(\vec{r}) = T_S(\vec{r}). \tag{21}$$

On the free surface of the melt and the external surfaces of the crystal, where heat is transferred by radiation,

$$k_m \frac{\partial T}{\partial n} = q_S(\vec{r}) \quad \text{on the melt surface,} \tag{22}$$

$$k_s \frac{\partial T}{\partial n} = q_S(\vec{r}) \quad \text{on the crystal surfaces.} \tag{23}$$

Here, $T_S(\vec{r})$ and $q_S(\vec{r})$ are the temperature and the outgoing heat flux on the skeleton of the global domain, respectively. On the melt–crystal interface, the following relationship should be satisfied:

$$k_m(\nabla T)_m \cdot \vec{n} = k_s(\nabla T)_s \cdot \vec{n} + \rho_s V_g \Delta H \vec{e}_z \cdot \vec{n}. \tag{24}$$

Heat is transferred in all solid macro-elements by conduction. The heat transfer in the heater is governed by

$$\nabla \cdot (k_h \nabla T) + S_Q = 0, \tag{25}$$

where S_Q is the heat source per unit volume in the heater. It is uniformly distributed in the heater and determined by the input heater power.

The governing equations for the thermal fields in other solid conductive macro-elements are in the form

$$\rho_i c_i \vec{V}_i \cdot \nabla T = \nabla \cdot (k_i \nabla T), \tag{26}$$

where $\vec{V}_i$ is the advection velocity. These solid macro-elements include the crucible, puller/seed, pedestal and heat insulators. The steel walls of the chamber are taken as a special solid conductive macro-element, in which the temperature is uniformly imposed with the temperature of the coolant flowing outside the thin walls.

On the inside wall of the heater and all conductive interfaces, condition (21) is applied. On the other radiative surfaces, the following condition is enforced:

$$k_i \frac{\partial T}{\partial n} = q_S(\vec{r}). \tag{27}$$

Finite volume calculations were carried out for the thermal fields in these macro-elements with a discretization on non-orthogonal grids.

5. Global solution

The global solution is obtained by solving the respective macro-elements separately and coupling them together. In other words, local iterations in each macro-element in the growth furnace and a conjugated global iteration among them constitute global modeling. In this section, we introduce conjugated global iteration in which all macro-elements are coupled with each other through appropriate treatment of the thermal conditions on the skeleton of the global domain and updates of unknown parameters of the system, i.e., the heater input power and melt–crystal interface.

5.1. Treatment of the thermal conditions on the skeleton of the global domain

Different macro-elements in a growth furnace are associated with each other through their interfaces that form the skeleton of the global domain. Effective and efficient treatment of the interfacial conditions on the skeleton is therefore important for global modeling. In our model, the thermal field on the skeleton of the global domain is kept fixed during the procedure for obtaining local solutions of respective macro-elements. It is renewed only in the global iteration according to the conditions: (1) the temperature is continuous across the interfaces and (2) energy balance is ensured at the interfaces. For the sake of clarity, we divide the skeleton into two types of interfaces: radiative interfaces that link a radiative enclosure and a solid conductive macro-element or the melt–crystal macro-element, and the conductive interfaces that link a solid conductive macro-element and another solid conductive macro-element or the melt–crystal macro-element.

The inside walls of the chamber are a special kind of radiative interface, on which the temperature is imposed with the coolant temperature. The heat flux is calculated in the local solution of the adjacent radiative enclosure by Eq. (5), i.e.,

$$q_S(\vec{r}) = q_{rad}(\vec{r}). \tag{28}$$

On the heater inside wall, we handle the thermal conditions with

$$T_S(\vec{r}) = T_{rad}(\vec{r}), \tag{29}$$

$$q_S(\vec{r}) = k_h \frac{\partial T}{\partial n}. \tag{30}$$

On the other radiative interfaces, the temperature is renewed as

$$T_S(\vec{r}) = T_{cnd}(\vec{r}). \tag{31}$$

The heat flux is renewed by expression (28). The subscript cnd represents the solution of a conductive macro-element or the melt–crystal macro-element, while rad represents the solution of a radiative enclosure. Because the mechanism of heat transfer in a CZ furnace and the system of governing equations are highly nonlinear, a relaxation technique is applied in renewing the thermal field on these interfaces. Relaxation parameter values between 0.05 and 0.3 are used in our calculations.

On a conductive interface between two 2D-featured macro-elements or between two 3D-featured macro-elements, the following relationships hold:

$$T_{i1}(\vec{r}) = T_{i2}(\vec{r}) = T_S(\vec{r}), \tag{32}$$

$$\left(k\frac{\partial T}{\partial n}\right)_{i1} = \left(k\frac{\partial T}{\partial n}\right)_{i2}, \tag{33}$$

where the subscript i is the interface index, 1 and 2 denote the macro-elements on both sides of the interface. On a conductive interface between a 2D-featured macro-element and a 3D-featured macro-element, the following two relationships hold:

$$T_{i1\in\partial V^2}(s') = T_{i2\in\partial V^3}(s',\theta) = T_S(s'), \tag{34}$$

$$\left(k\frac{\partial T}{\partial n}\right)_{i1\in\partial V^2} = \frac{1}{2\pi}\int_0^{2\pi}\left(k\frac{\partial T}{\partial n}\right)_{i2\in\partial V^3} \mathrm{d}\theta^*, \tag{35}$$

where s' is the longitudinal coordinate of the circumferential projection of the interface.

With this treatment of the thermal conditions on the skeleton of the global domain, local solutions of all macro-elements are conjugated with each other and the equation system of the problem is well closed. The principles of temperature continuity and energy balance across all of the interfaces are well satisfied when the global iteration is converged.

5.2. Determination of heater input power and melt–crystal interface location

The code requires only a set of input parameters to perform a global simulation by this model. These input parameters are the furnace geometry, material properties of each component, coolant temperature, melt volume, crystal radius and crystal growth rate. The heater input power and the melt–crystal interface shape are unknowns. They are solved iteratively in the global solution.

The intersection edge of the melt, crystal and gas, i.e., the tri-junction edge, is fixed in space. The temperature along the tri-junction edge, which is part of the skeleton of the global domain, is calculated from the equation system. In 3D global modeling with the assumption of axisymmetric geometry, the temperature along the tri-junction edge is not perfectly uniform. For the sake of clarity, let $\overline{T}_{tri}$ denote the current mean temperature over it. The heater input power is thus determined in such a way that it is modified iteratively in the global iteration according to $(T_m - \overline{T}_{tri})$ until $\overline{T}_{tri}$ approaches T_m. The mean temperature over the tri-junction edge is equal to the melting point of silicon when the global solution is converged.

The melt–crystal interface shape is three-dimensional. Its location is determined in such a way that it is updated iteratively in the global iteration according to $(T - \overline{T}_{tri})$, where T is the current local temperature on the interface, until $(T - \overline{T}_{tri})$ approaches zero. That is, we track the melt–crystal interface with identification to an isothermal face of the mean temperature over the tri-junction edge. Since the temperature cannot be perfectly uniform in the region of the interface near the tri-junction edge in this model, it is presumed to be smoothly distributed in this region. Thus, when the global solution is converged, the melt–crystal interface converges to an isothermal face of the melting temperature of silicon except a narrow region near the tri-junction edge where the temperature is smoothly distributed.

5.3. Global iteration strategy

In view of the extreme complexity and the high nonlinear property of the system, very small relaxation factors have to be adopted in the global solution, for example, in the skeleton treatment and in the heater power renewal process, if the 3D global iteration starts on the basis of a poor initial condition. The computation will thus be very time-consuming. In order to solve this problem, a 2D global simulation, which can be completed in a short computation time, is carried out at the outset for obtaining the initial fields in the furnace and the initial value of heater input power. Based on the 2D global solution, much larger relaxation factors can then be used in the 3D global iteration, resulting in a dramatic decrease in computation time.

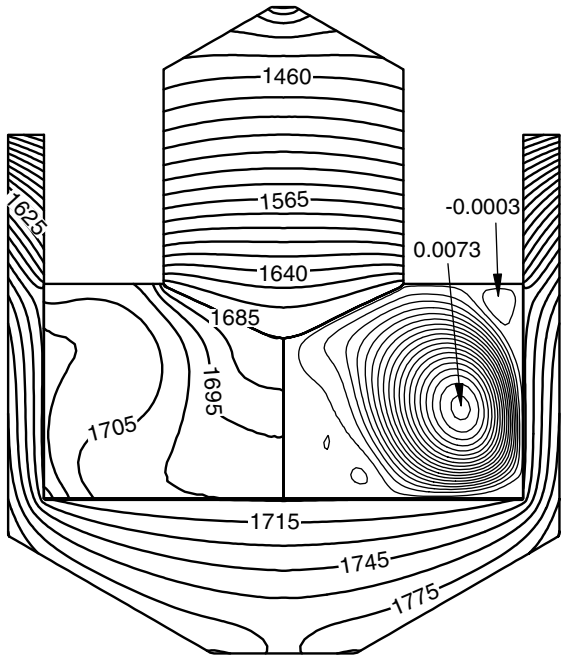

Fig. 3. Local temperature distribution, stream function distribution of melt flow and melt–crystal interface shape of a growth process with rotating crystal and crucible. Isotherms are plotted every 15 K in solids and every 5 K in the melt. The interval of stream function is 2×10^{-4} m^3/s.

The iteration procedure of the global solution is outlined as follows. (1) Carry out a 2D global simulation. The solution is taken as the initial field, the initial melt–crystal interface position and the initial value of the heater power for the following 3D global iteration. (2) Solve the melt flow, thermal field and external field, if it is imposed, in the melt–crystal macro-element with a fixed interface shape. (3) Solve the thermal fields in all of the other solid conductive macro-elements. (4) Renew the thermal field on the skeleton of the global domain according to Eqs. (30)–(33). (5) Calculate the radiative heat transfer in all radiative enclosures. (6) Renew the thermal field on all radiative surfaces according to Eqs. (28) and (29). (7) Check the convergence of the

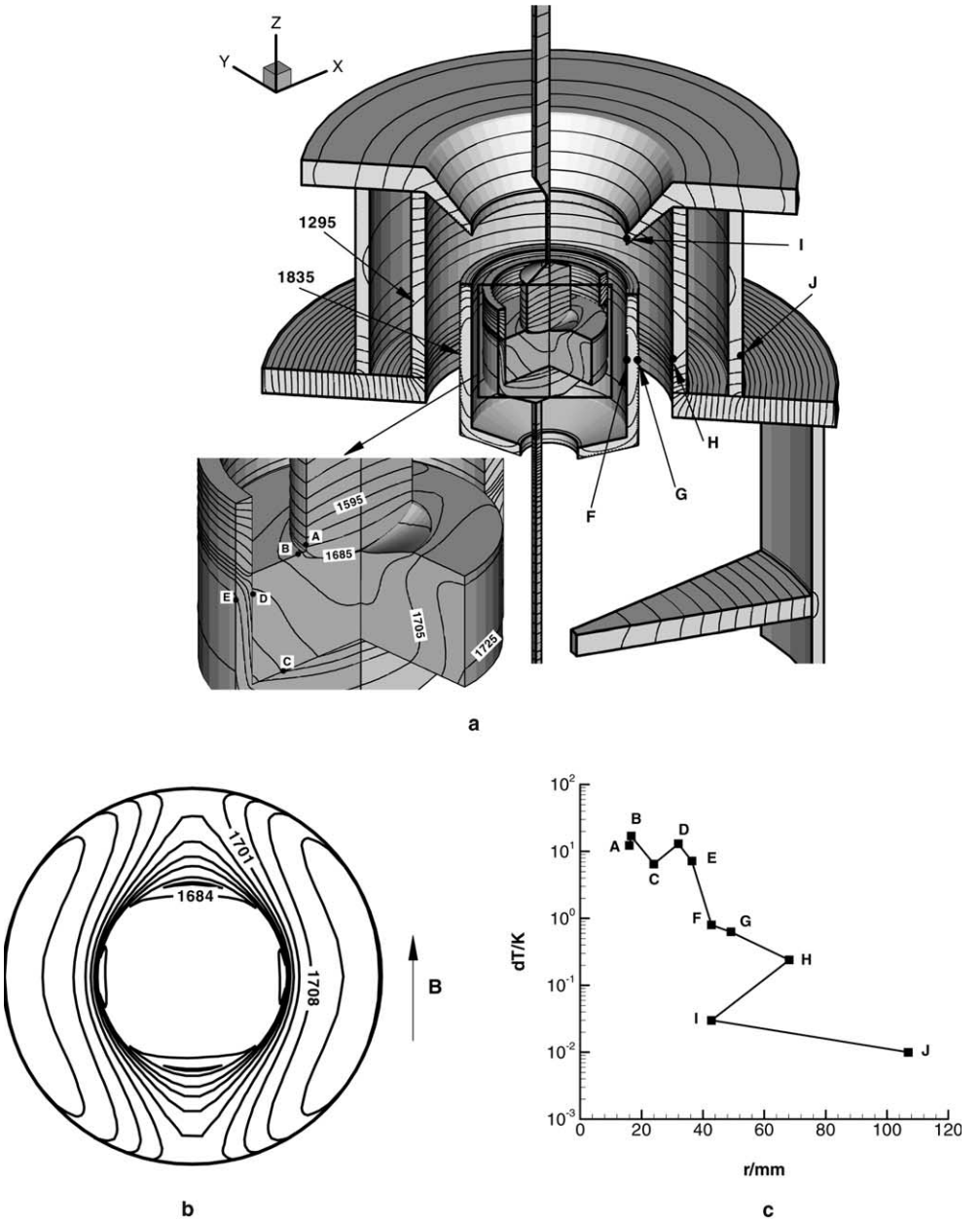

Fig. 4. Temperature distribution in a furnace in a transverse magnetic field. (a) Temperature distribution in the furnace and locations under consideration. Isotherms are plotted every 30 K in solids and every 10 K in the melt. (b) Temperature distribution at the melt top surface. Isotherms are plotted every 3.5 K. (c) Temperature differences over circumference at different locations.

global iteration. If it has not converged, return to step (2). If it has converged, proceed to step (8). (8) Check the convergence of the heater input power. If it has not converged, renew it according to $(T_m - \overline{T}_{tri})$ and then return to step (2). If it has converged, proceed to step (9). (9) Check the convergence of the melt–crystal interface location. If it has not converged, modify it according to $(T - \overline{T}_{tri})$. Adjust the computation grids in the melt–crystal domain to fit the new interface shape. Then return to step (2). If it has converged, terminate the computation and output the converged solution.

6. Computation results for model validation

Two test growth processes were numerically simulated to demonstrate the validity of the proposed model. The configuration of the growth furnace is as shown in Fig. 1(a). The diameters of the crystal and crucible are respectively 64 mm and 32 mm. All the components of the furnace were included in the 2D domain for a test growth process with a crystal rotating at 10 rpm and a crucible rotating at −3 rpm. The computation took about 34 h on a Pentium-4 PC machine. Fig. 3 shows the calculated results of temperature distribution in the crystal, melt and crucible. The stream function distribution of the melt flow is shown in the right half-plane of the melt region. The melt–crystal interface profile corresponds to the isotherm of 1685 K, the melting temperature of silicon. These results are in agreement with our previous analysis of the same growth furnace by a FEMAG analysis tool [11].

Another test growth process is in a transverse magnetic field with non-rotating crystal and crucible. The magnetic field is applied in the x-direction with an intensity of 0.3 T. The crystal, melt, crucible, heater and heat insulators were included in the 3D domain. The computation took about 42 days on a HP ITANIUM-2 workstation. Fig. 4(a) shows the temperature distributions in the melt as well as in solid components in the furnace. Three-dimensional features can be obviously seen in the core region of the furnace, especially in the melt. The temperature distribution at the melt top surface is presented in Fig. 4(b). It can be noticed that it is prominently non-uniform in the azimuthal direction. In order to check the temperature non-uniformity over circumference in the furnace, some representative locations (point A through point J) were selected for consideration, as shown in Fig. 4(a). The temperature differences over circumference at these locations were compared in Fig. 4(c). It is found that the temperature difference decreases rapidly with distance away from the melt region. It remains prominent even at the outside wall of crucible. However, in the heat insulators that are away from the melt region, the temperature distribution is rather uniform in the azimuthal direction. This means that the core region of the furnace must be treated in 3D but the heat insulators away from the core region can be treated in 2D in order to save computation resources, demonstrating that the proposal of 2D domain and 3D domain in establishing our 3D global model is reasonable.

The melt–crystal interface shape was found to be 3D in this growth process, which can be observed in Fig. 4(a). In Fig. 5, a top view of the interface with identification to the isothermal surface of the melting temperature of silicon is shown. These results are in good agreement with the experimental research of Kajigaya et al. [12]. In their experiment, ellipsoid crystals with 3D interface shapes were grown in a transverse magnetic field with the same intensity under a condition without seed rotation.

To determine which components should be included in the 3D domain is important for computation accuracy in this model. In order to investigate the dependence of the choice of components included in the 3D domain on the temperature field in the melt, other three choices of components in the 3D domain were investigated for comparison: the first choice with the crystal, melt, crucible and heater in the 3D domain, the second choice with the crystal, melt and crucible in the 3D domain and the third choice with the crystal and melt only in the 3D domain. The comparison investigation revealed that, the difference between the results of the first choice and the results shown in Fig. 4 is negligible. The difference between the results of the second choice and the results shown in Fig. 4 is also small. However, the results of the third choice are obviously different from that shown in Fig. 4. For comparison, Fig. 6 shows

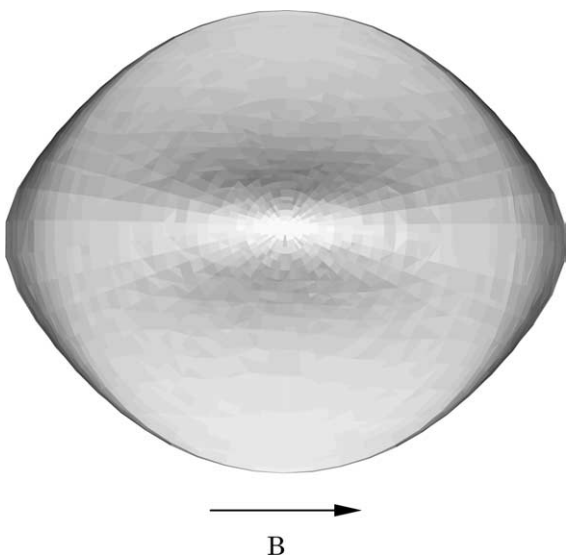

Fig. 5. Top view of the melt–crystal interface.

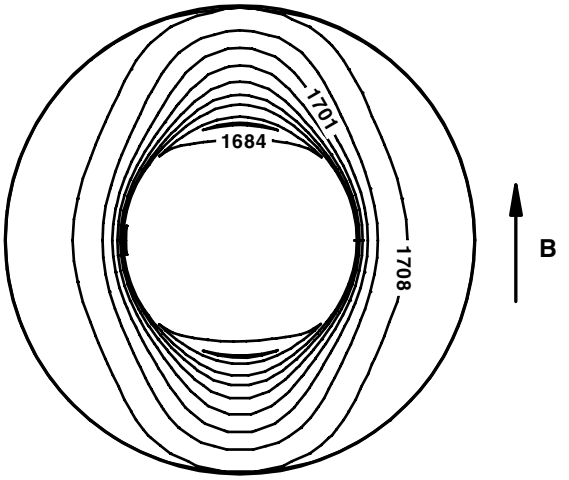

Fig. 6. Temperature distribution at the melt top surface in the case with the melt–crystal macro-element only included in the 3D domain. Isotherms are plotted every 3.5 K.

the temperature distribution at the melt top surface that was obtained from the modeling in which only the melt and crystal were included in the 3D domain. The comparison shows that the crucible should be included in the 3D domain in the modeling. The comparison investigation further demonstrates the validity of the proposed model.

7. Conclusions

A three-dimensional global model for silicon CZ furnaces was proposed. The modeling involves accurately solving the thermal fields in all constituents and the 3D radiative heat transfer in the furnace with a set of control parameters. A mixed 2D/3D discretization scheme was developed, and the concepts of 2D domain and 3D domain were introduced. 3D global modeling is feasible with moderate requirements of computer memory and computation time using this model. The code of this model has good adaptability for any 3D-featured CZ growth process with easy adjustment of the interface location of the 2D domain and the 3D domain in accordance with available computer resources and permissible computation time. The model can also be extended to fully 3D global modeling or 2D global modeling. The global iteration algorithm is stable, though the system is extremely nonlinear. The validity of the model was demonstrated.

Acknowledgement

This work was supported by a Grant-in Aid for Scientific Research (B) 14350010 from the Japanese Ministry of Education, Science, Sports and Culture.

References

[1] N. Kobayashi, Computational simulation of the melt flow during Czochralski growth, J. Cryst. Growth 43 (1978) 357–363.
[2] A. Krauze, A. Muiznieks, A. Muhlbauer, Th. Wetzel, W.v. Ammon, Numerical 3D modelling of turbulent melt flow in a large CZ system with horizontal DC magnetic field. I: Flow structure analysis, J. Cryst. Growth 262 (2004) 157–167.
[3] K. Kakimoto, L.J. Liu, Numerical study of the effects of cusp-shaped magnetic fields and thermal conductivity on the melt–crystal interfaces in CZ crystal growth, Cryst. Res. Technol. 38 (7–8) (2003) 716–725.
[4] J.J. Derby, R.A. Brown, Thermal-capillary analysis of Czochralski and liquid encapsulated Czochralski crystal growth: I. Simulation, J. Cryst. Growth 74 (1986) 605–624.
[5] L.J. Atherton, J.J. Derby, R.A. Brown, Radiative heat transfer in Czochralski crystal growth, J. Cryst. Growth 84 (1987) 57–78.
[6] F. Dupret, P. Nicodeme, Y. Ryckmans, P. Wouters, M.J. Crochet, Global modelling of heat transfer in crystal growth furnaces, Int. J. Heat Mass Transfer 33 (9) (1990) 1849–1871.
[7] M. Li, Y. Li, N. Imaishi, T. Tsukada, Global simulation of a silicon Czochralski furnace, J. Cryst. Growth 234 (2002) 32–46.
[8] V.V. Kalaev, I.Yu. Evstratov, Yu.N. Makarov, Gas flow effect on global heat transport and melt convection in Czochralski silicon growth, J. Cryst. Growth 249 (1–2) (2003) 87–99.
[9] K. Koai, A. Seidl, H.-J. Leister, G. Müller, A. Kohler, Modelling of thermal fluid flow in the liquid encapsulated Czochralski process and comparison with experiments, J. Cryst. Growth 137 (1994) 41–47.
[10] V.V. Kalaev, D.P. Lukanin, V.A. Zabelin, Yu.N. Makarov, J. Virbulis, E. Dornberger, W. von Ammon, Calculation of bulk defects in CZ Si growth: Impact of melt turbulent fluctuations, J. Cryst. Growth 250 (2003) 203–208.
[11] K. Kakimoto, P. Nicodeme, M. Lecomte, F. Dupret, M.J. Crochet, Numerical simulation of molten silicon flow: Comparison with experiment, J. Cryst. Growth 114 (1991) 715–725.
[12] T. Kajigaya, T. Kimura, Y. Kadota, Effect of the magnetic flux direction on LEC GaAs growth under magnetic field, J. Cryst. Growth 112 (1991) 123–128.